Medical Engineering and Physics 63 (2019) 33–41

Contents lists available at ScienceDirect

Medical Engineering and Physics

journal homepage: www.elsevier.com/locate/medengphy

Finite element analysis of knee and ankle joint during gait based on motion analysis

Sangbaek Park, Seungju Lee, Jeongro Yoon, Soo-Won Chae*

Department of Mechanical Enginnering, Korea University, 145, Anam-ro, Seongbuk-gu, Seoul 02841, Republic of Korea

ARTICLE INFO

Article history:
Received 18 October 2017
Revised 22 October 2018
Accepted 5 November 2018

Keywords:
FE analysis
Contact pressure distribution
Knee and ankle
Dynamic analysis
Gait

ABSTRACT

Contact pressures in the articular cartilage during gait affect injuries and the degenerative arthritis of knee and ankle joints. However, only contact forces at the knee and ankle joints during gait can be estimated by using a rigid body dynamic model. The contact pressure distribution can be obtained quantitatively for a static posture by using finite element (FE) analysis in most cases. The purpose of this study is to develop a new method to obtain the contact pressure distribution at the knee and ankle joints during gait by integrating FE analysis with rigid body dynamic analysis. In this method, a reference FE model of the lower extremity is constructed first and is then transformed to each stance phase of the gait obtained from dynamic analysis by using homogeneous transformation. The muscle forces and ground reaction force (GRF) during gait obtained from the dynamic analysis were used as loading conditions for FE analysis. Finally, the contact pressure distribution at the tibia plateau cartilage and talus cartilage were estimated at the 1st peak, mid-stance, and the 2nd peak at the same time. The present method can provide the contact pressure distribution at the knee and ankle joints over the entire gait.

1. Introduction

The lower extremity, which is responsible for supporting the entire body, is subject to various loads during motion. In particular, the knee and ankle are prone to sports-related injuries and diseases such as osteoarthritis. Much research effort has been made on analyzing the biomechanical behaviors of the lower extremity during motion. Research using dynamic simulation software such as OpenSim [1], LifeMod [2], and AnyBody [3] has been frequently employed only to obtain contact forces and muscle forces. Liu et al. [4] studied muscle activation according to the range of walking speed to confirm the muscle contributions obtained from OpenSim. Kia et al. [5] evaluated the contact force at the knee joint as well as the GRF with a musculoskeletal model through gait trials using LifeMode. Wang et al. [6] analyzed knee contact forces to research the influence of gait speeds using Anybody. Research without using dynamic simulation software has also been performed. Simic et al. [7] and Taniquchi et al. [8] analyzed joint moment or power by using dynamic analysis according to the changes in gait patterns or shoes. However, these studies were limited to investigations of kinetic or kinematic effects and accurate contact pressure distributions at the knee and ankle joints could not be obtained [9,10].

Some FE analyses related to gait have been performed to obtain the contact pressure distribution. However static or quasi-static analyses were mainly performed without considering dynamic characteristics [11–15]. Gefen et al. analyzed the gait phase through quasi-static FE simulations [16]. Simulation sets for each stance phase were constructed according to the angles between the ground and foot from fluoroscopy during gait without considering joint angles. Gefen studied the foot except for the knee and the inertia force was considered. Other foot models were used in studies conducted by Cheung et al. [11–14], in which the effects of various insoles were analyzed. In Cheung's studies, static analysis was conducted only in the standing posture, and changes in posture and muscle forces during motion were not considered. Donahue et al. [17] analyzed knee contact behavior using an FE model, but the joint motion of the knee was not considered. Penrose et al. [18] verified the gross kinematic response of knees in diverse biomechanical situations, although the muscles of the lower limb were simplified. Using a knee-ankle-foot complex model, Liu and Zhang [15] evaluated the effect of laterally wedged insoles on the stress distribution at the knee. The researchers evaluated the knee-ankle-foot complex model for a single stance in a quasi-static manner.

The objective of this study is to develop a new method that integrates FE analysis with rigid body dynamic analysis to obtain the contact pressure distributions at the knee and ankle joints during gait.

* Corresponding author.
E-mail address: swchae@korea.ac.kr (S.-W. Chae).

https://doi.org/10.1016/j.medengphy.2018.11.003
1350-4533/

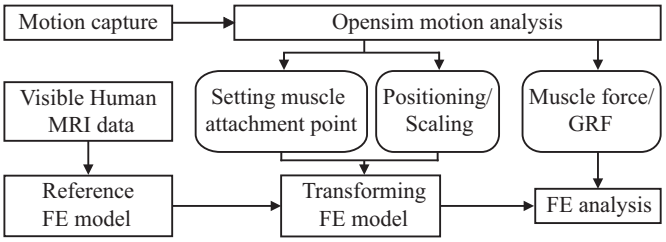

Fig. 1. Workflow of present method.

2. Method

The workflow of the present method is presented in Figure 1. The geometry data of the lower extremity were obtained from Visible Human MRI data. Initially, a reference FE model was constructed to match the coordinate, size and position of the dynamic model. Motion was captured experimentally for a normal gait and motion analysis was conducted with this motion data. Motion capture data were used to transform the reference FE model to corresponding positions during gait and to apply them to the FE model for analysis.

2.1. FE model

In the present study, a lower extremity FE model was constructed for a knee-ankle-foot complex, ranging from femur to foot (Fig. 2). Employing MRI data provided by the Visible Human Project [19], the 3D geometry of the femur, tibia, fibula, patella, foot segments, articular cartilages and meniscus were reconstructed using Mimics (Materialise, Ann Arbor, MI).

The bones consisted of the femur, patella, tibia, fibula and 25 foot bones. These were modeled with three-node shell elements. Since the deformation of bones during normal gait is usually very small, the bone FE models were assumed as rigid bodies.

The cartilage, meniscus, and meniscus horn model was constructed with solid eight-node hexahedral elements using Hypermesh 13.0 (Altair Engineering, Troy, MI, USA) (Fig. 2(b)). A solid eight-node hexahedral element (C3D8R) was used to apply linearly varying properties to the depth of the tibia plateau cartilage and to set the material property of the meniscus to transversely isotropic linear elastic. The element size/mesh density for each structure (articular cartilage and meniscus) was adopted by referencing the mesh convergence analyses of a previous study [20]. That is, about 2100 elements were used in the meniscus, 4900 for the femur cartilage, 3600 for the tibia cartilage, and 1650 hexahedral elements for the talus cartilage. The properties of the major ligaments of the knee and ankle are listed in Table 1 [21–26]. The insertion points of the ligaments were determined to a specific node of the shell element of the bone based on anatomy [27]. The muscle attachment points were defined to a specific node of the shell element of the bone according to the OpenSim coordinates.

Femur articular cartilages and Tibia plateau cartilages were modeled as isotropic linear elastic material with three layers. Young's modulus was set to 10 MPa, 14 MPa and 18 MPa from the surface layer to the deep zone layer, and Poisson's ratio was 0.49 [28]. In the ankle joint, the tibia and talus articular cartilages were modeled as linear elastic material with a Young's modulus of 12 MPa and Poisson's ratio of 0.45 [29]. The meniscus were modeled as transversely isotropic linear elastic material in the axial and radial directions with a Young's modulus of 20 MPa and Poisson's ratio of 0.3. In the circumferential direction, Young's modulus 120 MPa, and Poisson's ratio 0.45. The meniscus horns were modeled as isotropic linear elastic material with a Young's modulus of 111 MPa and Poisson's ratio of 0.49 [20].

Table 1
Material properties of ligaments.

	Stiffnes (N/mm)
CFL, TICL	126.6
PTiTL	244.3
ATiTL	122.3
ATFL	141.8
ACL	201
PCL	258
LCL	2114
MCL	134

CFL: CalcaneoFibular Ligament, TICL: TibioCalcaneal Ligament, PTiTL: Posterior TibioTalus Ligament, ATiTL: Anterior TibioTalus Ligament, ATFL: Anterior TaloFibular Ligament, PCL: Posterior Cruciate Ligament, ACL: Anterior Cruciate Ligament, LCL: Lateral Collateral Ligament, MCL: Medial Collateral Ligament.

2.2. Coordinate system matching between OpenSim and FE model

In this study, an interface program with self-written codes was developed to apply the results of a motion analysis to the FE analysis. The motion analysis was conducted by using OpenSim 3.2 (Simbios, Stanford, CA, USA), and the FE analysis was conducted by using ABAQUS 6.13 (SIMULIA, Providence, RI). The initial marker positions obtained from the motion capture system were used in calculating the scale factors for matching the OpenSim and reference FE model to the subject. Next, marker trajectory data were obtained through motion capture, and the angle of each joint was calculated in OpenSim. These values were used to rearrange the FE part models according to the captured posture. Ligament elements were modeled as truss elements connecting the predefined attachment point of the rearranged FE model. These truss elements were assumed to have no-initial-pre-strains material properties.

The FE model should be converted to match the coordinates of the Gait2354 model, which is a basic simulation model in OpenSim, because the joint definitions in OpenSim should be applied to the FE model. Based on previous studies [30,31], the joint and the center of motion were defined in the FE model. After the joint positions of the FE model were defined, the reference FE model was divided into five models according to the segment bodies of the OpenSim model: toe body model, calcaneus body model, foot body model, tibia body model, and femur body model. Each FE model was aligned according to the joint position definition of the OpenSim model. Based on the distance between the joint positions, OpenSim base model was scaled to the same size as the participant used for motion analysis. Each FE model was also resized to the same size as the scaled OpenSim model by linear scaling. The resizing parameters used were 0.943 for pelvis, 0.983 for femur, 0.973 for tibia and 0.974 for foot.

It was assumed that the muscle force provided tension between two attachment points of each muscle. Then, forces were applied at each pre-determined attachment point of the FE model as a pair of point forces. The magnitude of the muscle forces was estimated by using the computed muscle control of the OpenSim. The direction of muscle force was referred to the direction of the muscle path of the Gait2354 model. A total of 10 muscle forces, which occurred in the biceps femoris long head, biceps femoris short head, tensor fasciae latae, gracilis, rectus femoris, vastus intermedius, medial gastrocnemius, soleus, tibialis posterior, and tibialis anterior muscle, were applied. Among these muscles, four major muscle activations were presented as graphs (Fig. 3).

Cross-correlation analyses were used to quantify the muscle activation between our study and previous study [32] on EMG.

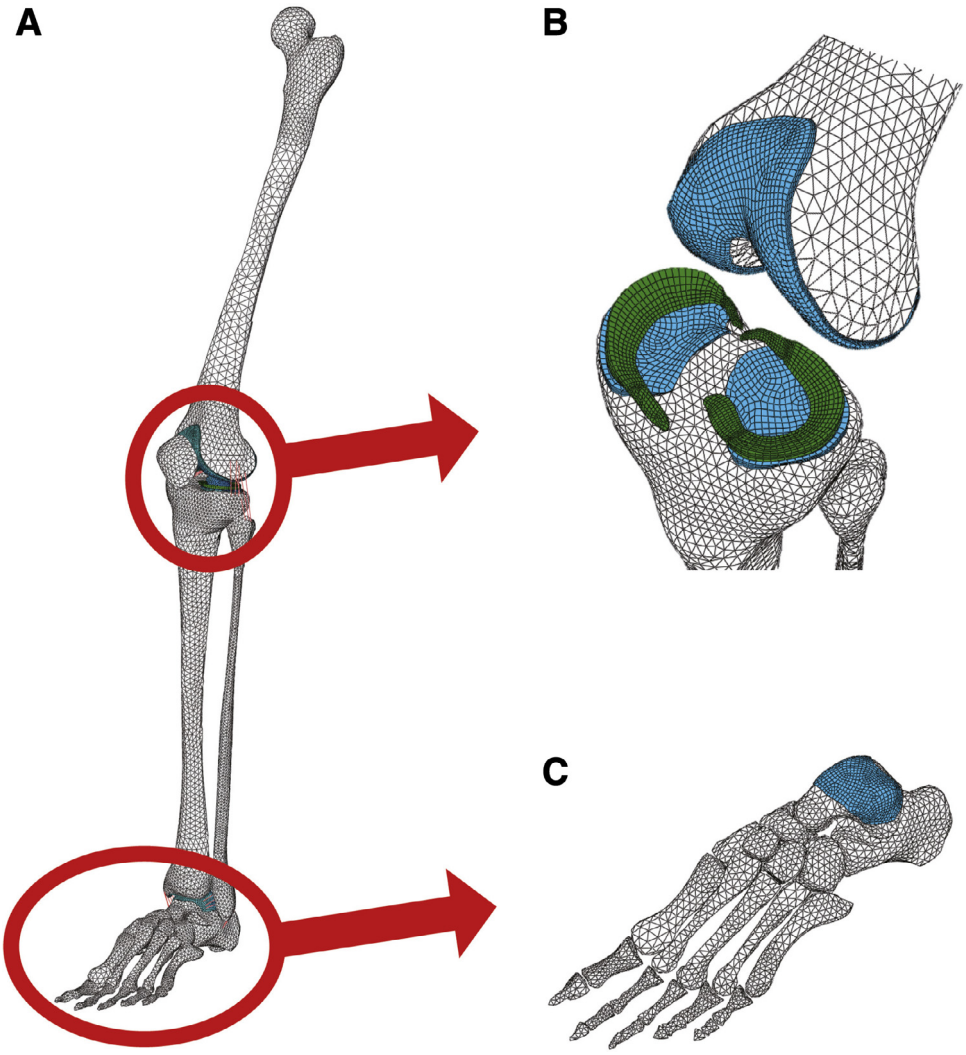

Fig. 2. FE model with bones and cartilage (A) lower extremity model, (B) knee region and (C) foot region.

Cross-correlation quantifies the similarity in shape and muscle activation data [33–37]. Cross-correlation analyses were performed using Matlab R2006a version 7.2 (The Mathworks, Inc., Natick, MA, USA) with the following equation

$$R_{xy}(\Delta) = \frac{\int x(t)y(t+\Delta)dt}{\sqrt{\int x^2(t)dt \int y^2(t)dt}} \quad (1)$$

where x and y are the two waveforms and Δ is the time lag between the two signals. A highly positive correlation is an indication that the two signals are very similar. So, the muscle activations of our study and that of the previous study were compared with the EMG signals of the previous study, respectively. The correlation coefficients of the previous study and the our study were 0.685 and 0.605 for Biceps Femoris Long Head, 0.872 and 0.934 for Soleus, 0.771 and 0.840 for Rectus Femoris and 0.747 and 0.594 for Tibialis Anterior, respectively. In the case of Soleus and Rectus Femoris, muscle activation in this study is quantitatively similar to EMG in the previous studies. In the case of Becips Femoris Long Head, the correlation coefficient is slightly lower than the previous study. There is a difference in the time delay between the previous study and the present study. The error is caused by differences in the number of muscles used in the analysis. In the case of Tibialis anterior, the correlation coefficient is lower than the previous study. There is an error in the swing phase after 60% of cycle but it does not affect the joints more than the stance phase. In addition, the muscle activation increases at 30% and 50%, which appears to be an antagonist to Soleus activation errors.

The attachment point of the Quadriceps muscle is defined as the position of the moving point according to knee angle with respect to tibia frame for simplified calculation in OpenSim model. Thus, we defined the location of the patella on tibia frame so that the quadriceps muscle attachment point of the patella coincides with the moving point.

A homogeneous transformation was employed to transform the FE model [38]. The lower extremities of OpenSim model has six parent-child couples; ground(global)-pelvis, pelvis-femur, femur-tibia, tibia-talus, talus-calcaneus, and calcaneus-toe. In FE modeling process, the pelvis was not considered. Since each child body is defined by a coupled parent body, the joint motion should be employed in the child body to transform the local coordinate to a global coordinate. Let ${}^{child}_{child}X$ be the node position of a child body before transformation. The transformed nodes with the joint motion of the child body can be expressed as ${}^{child}_{child}X'$. In addition ${}^{c}_{c}x_n$, ${}^{c}_{c}y_n$, and ${}^{c}_{c}z_n$ are the coordinates of the nth node in the child body

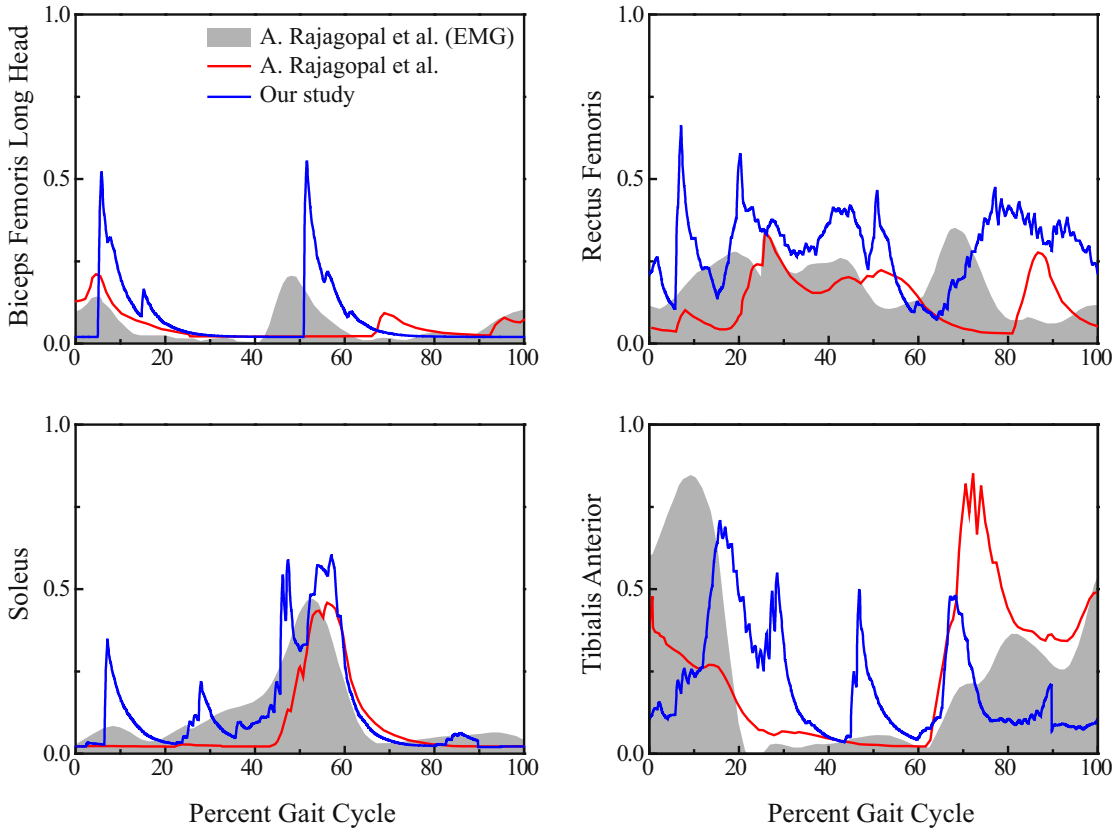

Fig. 3. The main muscle activations compared to the published data for the lower extremity muscles during gait. (Gray shaded regions: experimental EMG signals of previous study, red line: simulated muscle activity of the previous study, blue line: simulated muscle activity of our study.)

frame.

$$ {}^{child}_{child}X = \begin{bmatrix} {}^{c}_{c}x_1 & {}^{c}_{c}x_2 & \dots & {}^{c}_{c}x_n \\ {}^{c}_{c}y_1 & {}^{c}_{c}y_2 & \dots & {}^{c}_{c}y_n \\ {}^{c}_{c}z_1 & {}^{c}_{c}z_2 & \dots & {}^{c}_{c}z_n \\ 1 & 1 & \dots & 1 \end{bmatrix} \tag{2} $$

$$ {}^{child}_{child}X' = {}^{child}_{child}L \cdot {}^{child}_{child}X, \ where \ {}^{child}_{child}L = {}^{child}_{child}T \cdot {}^{child}_{child}R \tag{3} $$

In Eqs. (2) and (3), ${}^{child}_{child}T$ is the translational transformation matrix and ${}^{child}_{child}R$ is the rotational transformation matrix using the ZYX Euler angle convention in the child coordinate system (Fig. 4(a)). According to Briot and Khalil [39], the translational displacement $\boldsymbol{d}$, given by the vector

$$ \boldsymbol{d} = a\boldsymbol{i} + b\boldsymbol{j} + c\boldsymbol{k}, \tag{4} $$

can be described by the translational transformation matrix ${}^{child}_{child}T$

$$ {}^{child}_{child}T = Trans(a,b,c) = \begin{bmatrix} 1 & 0 & 0 & a \\ 0 & 1 & 0 & b \\ 0 & 0 & 1 & c \\ 0 & 0 & 0 & 1 \end{bmatrix} \tag{5} $$

After applying the joint motion to the child body model, the body should be expressed in the parent body frame. The coordinates of the nodes in the child body frame (tibia body frame) can be expressed as ${}^{child}_{parent}X'$ in the parent body frame (femur body frame).

$$ {}^{child}_{parent}X' = {}^{child}_{parent}L \cdot {}^{child}_{child}X', \ where \ {}^{child}_{parent}L = {}^{child}_{parent}T \cdot {}^{child}_{parent}R \tag{6} $$

In Eq. (6), ${}^{child}_{parent}L$ is the matrix that defines the relative coordinates of the child frame (tibia frame) in the parent frame (femur frame) (Fig. 4(b)). ${}^{child}_{parent}T$ is the translation matrix for the relative location along the vector from the parent frame to the child frame. ${}^{child}_{parent}R$ is the rotation matrix for the relative orientation between the two frames obtained by the direction cosine between the coordinate axes, where ${}^{c}x'$, ${}^{c}y'$, and ${}^{c}z'$ are locally transformed child frame coordinate axes, and ${}^{p}x$, ${}^{p}y$, and ${}^{p}z$ are parent frame coordinate axes. In this manner, along the parent-child tree, the coordinates in the local frame can be expressed in the global frame. The bodies in the lower extremity were dependent on the motion of their parent body (Fig. 4(c)). The global coordinates of all bodies could be obtained using Eq. (4) along the parent-child tree. Using the program developed in this study, the results of the OpenSim analysis were read and automatically employed in the FE model automatically. As a result, FE models at each stance phase of the gait could be prepared.

2.3. Motion analysis

A normal gait analysis was carried out for the validation. Motion capture to acquire the data of the gait motion was performed with a participant (male, 28 years old, 74 kg in weight, and 177 cm in height). A motion capture system (EGL-500-8 by Motion Analysis Corporation) was used in this study. The participant was free of disease and did not have any history of severe lower-limb injury. Korea University Institutional Review Board (IRB) approved this research (1040548-KU-IRB-15-263-A-1), and the participant provided written consent. A Plug-in-Gait marker set was used for data acquisition, and two force plates (AMTI's BP400600-2000) were placed under the path of the gait. Motion capture during walking at a naturally self-controlled pace while barefoot was performed. In this procedure, measurements were taken five times (Fig. 5). Among the five cases, the data closest to the average value in the

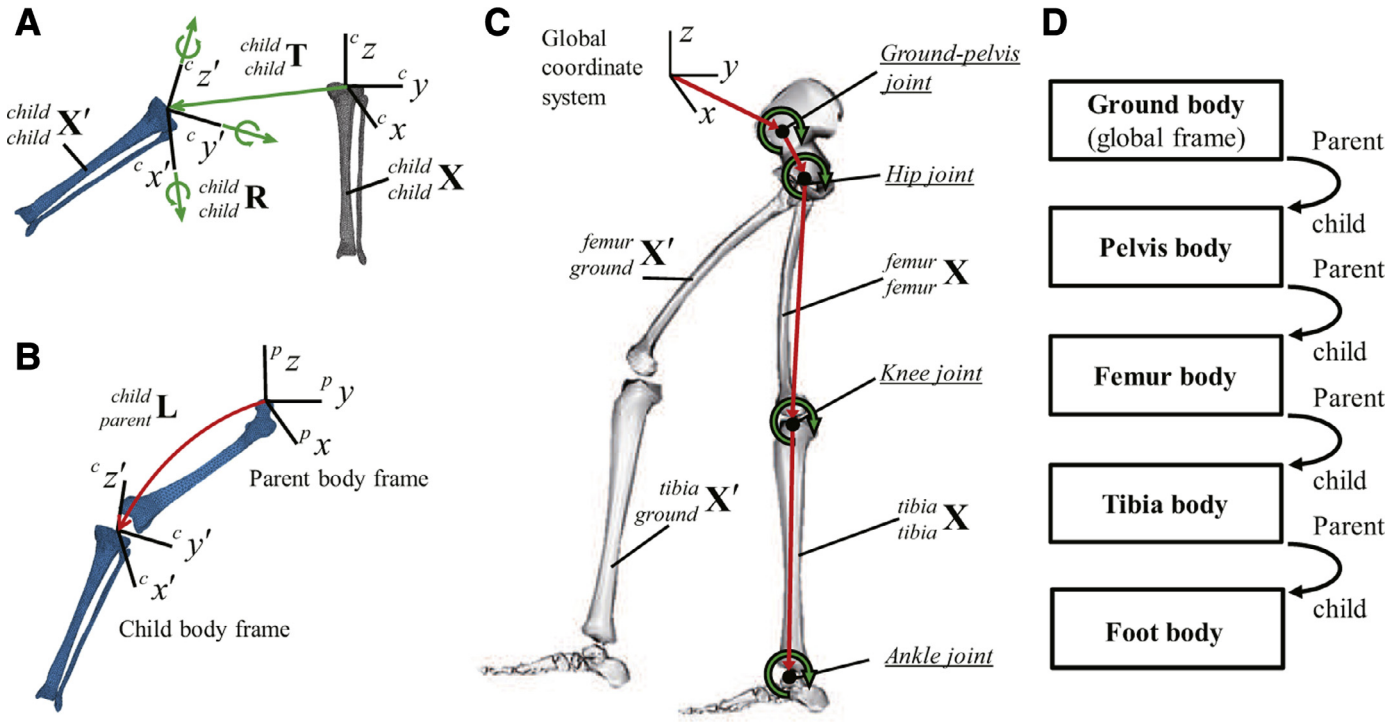

Fig. 4. Transformation of FE model: (A) transformation for joint motion based on child body (tibia) coordinate system, (B) relative position of child body in parent body (femur) coordinate system, (C) lower extremity model after and before transformation and (D) parent-child flow chart.

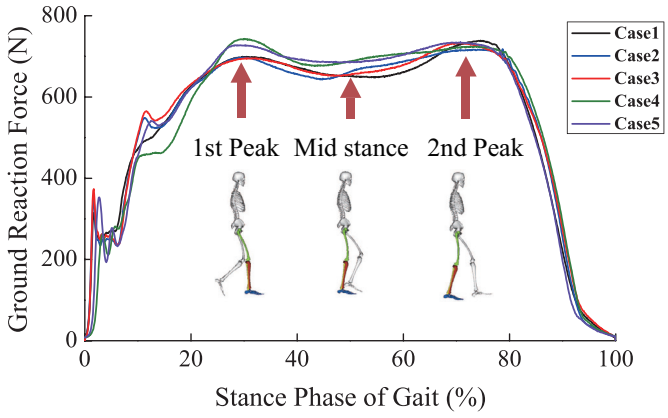

Fig. 5. Five cases of GRF and colored lower extremities indicating three gait postures according to stance phase of gait.

1st peak of GRF, mid-stance, and the 2nd peak of GRF were selected. The walking speed was recorded as 1.1 m/s. The marker trajectory data were converted into joint angles by using OpenSim and the joint angles were employed to adjust the FE model's posture at the major stance phases of the gait: the 1st peak of GRF, mid stance, and the 2nd peak of GRF.

2.4. FE model validation

In order to validate our FE model, the peak contact pressure and contact area at the knee and ankle joint obtained in the present study were compared with those of previous studies (Fig. 6). Previous studies provided peak contact pressure and contact area in tibia plateau cartilage of knee joint when 1000N compressive load was applied to the femur without muscle forces while tibia was fixed [40–46]. A peak contact pressure of 1.6 to 3.2 MPa and contact area of 1100 to 2000 mm^2 were reasonable. For the same boundary and loading conditions, the numerical values of our FE model were within these ranges since the peak contact pressure was 2.8 MPa and the contact area was 1640 mm^2. The peak contact pressure and contact area in the talus articular cartilage of the ankle joint were also obtained by Anderson et al. when a 600 N compressive load was applied to the tibia while the foot was fixed [29]. A peak contact pressure of 2.92 to 3.69 MPa and contact area of 295.1 to 493.6 mm^2 were reasonable. It is plausible that our FE model was well within the ranges since the peak contact pressure was 3.30 MPa and the contact area was 462.0 mm^2 for the same loading and boundary condition of Anderson's study.

Contact points in the femur cartilage according to the knee rotational angle (0°, 30°, 60°, and 90°) were also examined to verify the accuracy of the matched coordinate system. According to Li et al. [47], the centroid of the contact area was defined as a contact point. Our estimated contact points in the femur cartilage had a similar tendency (Fig. 7).

2.5. FE analysis

FE analyses were performed using the ABAQUS/Standard 6.13 (Static Analysis, SIMULIA, Providence, RI) program. In detail, the contact condition at the knee joint was used for three sets of master and slave: the femur cartilage and meniscus, femur cartilage and tibia plateau cartilage, and the tibia plateau cartilage and meniscus. For the ankle joint, the tibia cartilage and talus cartilage were set as contact pair. The normal behavior of a contact condition was set as a hard contact condition, and the tangential contact was assumed as a frictionless property. To optimize the computational expense, each foot segment (toe, calcaneus, and talus) and shank segment (tibia, fibula, and patella) were assumed as one rigid body. The center of each rigid body was set as a reference point, and the nodes of the cartilage surface adjacent to the bone were constrained to the reference points as tie conditions. The muscle forces obtained from OpenSim were applied as the loading conditions of the FE analysis. GRF data with the force

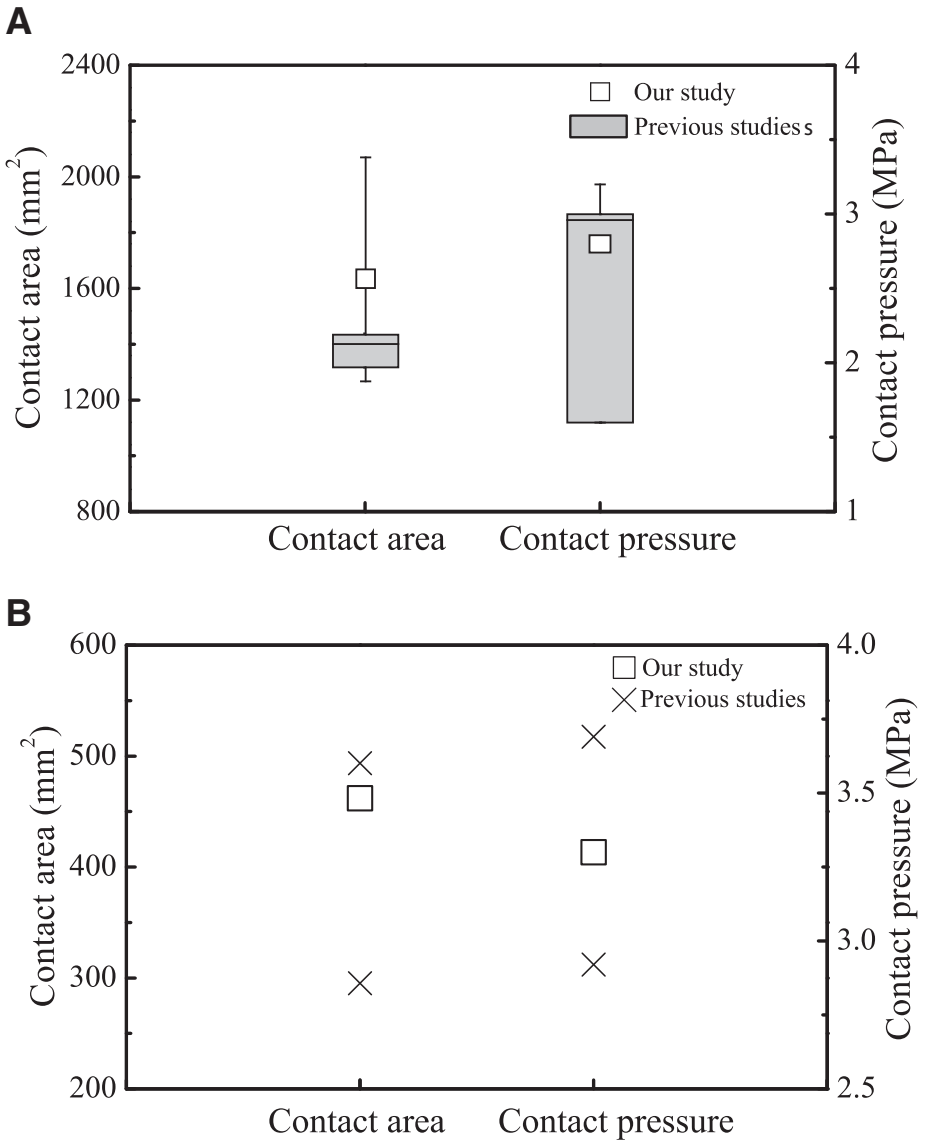

Fig. 6. Comparison of contact area and contact pressure between our study and previous studies: (A) 25th to 75th percentile with minimum and maximum of previous studies at knee joint, and (B) results of two previous study cases at ankle joint.

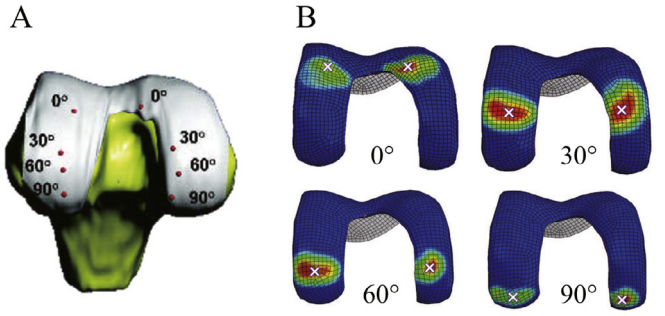

Fig. 7. Comparison of contact point of femur cartilage at 0°, 30°, 60° and 90° knee rotational angle. (A) Previous study and (B) our study. (Guoan Li et al., The American Journal of Sports Medicine, Vol. 33 Issue 1, pp. 102–107, Copyright ©2017 Copyright Clearance Center, Inc., reprinted by Permission of SAGE Publications, Inc.)

vector and the position were taken from the force plate and applied to the foot segments as external loads. The femur at each stance phase of the gait was fixed in all degrees of freedom (DOF) during analysis. In OpenSim, one rotational DOF for knee and two rotational DOFs for ankle were considered. Along with these rotational DOFs, all the other rotational DOFs were also constrained because knee and ankle rotations were taken from the OpenSim kinematics. Translational DOFs were not constrained.

3. Results

The net joint reaction forces in the knee and ankle were compared with those of the previous study [48]. The knee joint reaction forces were 1.65, 1.08 and 1.54 times the body weight (BW) at the 1st peak, mid-stance, and 2nd peak, respectively, and the ankle joint reaction forces were 1.14, 0.71, and 1.26 BW. These results are similar to those of the previous studies (1.74, 1.14, and 1.59 BW for the knee; 1.27, 0.76, and 1.20 BW for the ankle). The contact pressure distribution at the tibia plateau cartilage could be observed (Fig. 8). The peak contact pressure at the tibia plateau cartilage was 7.9 MPa at the 1st peak, 5.8 MPa at the mid-stance, and 6.2 MPa at the 2nd peak. The peak contact pressure at the tibia plateau cartilage was found to be higher at the medial side than at the lateral side. For the ankle, the contact pressure distribution at the articular cartilage of the talus was represented as shown in Figure 8. The

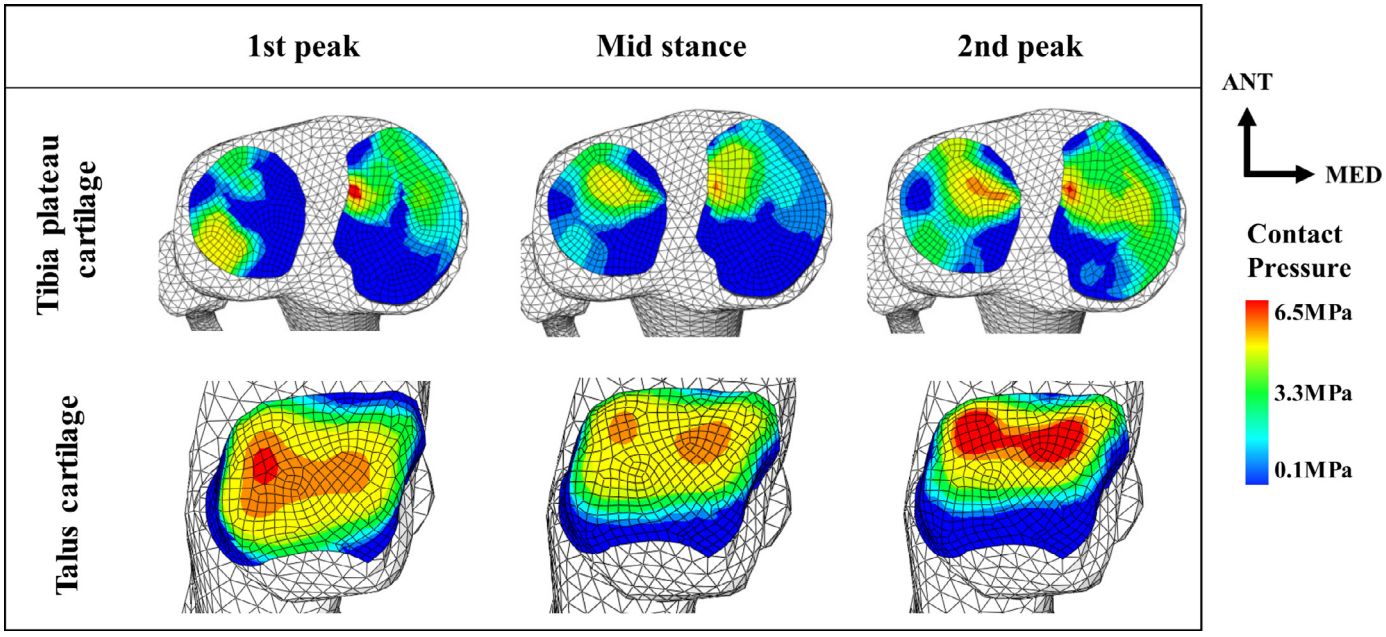

Fig. 8. Results of FE analysis: contact pressure distributions on tibia plateau cartilage and talus cartilage at 1st peak, mid-stance, and 2nd peak.

peak contact pressure of the talus cartilage was 6.6 MPa at the 1st peak, 5.9 MPa at mid stance, and 8.8 MPa at the 2nd peak. For the ankle, the location of the peak contact pressure was at the lateral cartilage of the talus. From the contact pressure distribution, it was also confirmed that the contact region in the talus cartilage moved to the anterior area as the stance phase proceeded from the 1st peak to the 2nd peak.

4. Discussions

The reference FE model employed in the proposed method was validated for peak contact pressure at the knee and ankle cartilage and for the contact point location according to the joint angle. The difference between absolute values seems to be caused by the geometrical differences in the biomechanical models. Generally, this type of limitation can be found in other studies using biomechanical models owing to the difficulties of in-vivo experiments.

In the present study, contact pressure distributions at the knee and ankle cartilage were obtained with respect to the 1st peak stance phase, mid-stance phase, and 2nd peak stance phase since the contact pressure at the cartilage is known to be a main factor in arthritis. However, in many studies that evaluated the effects of treatments on arthritis with medical aids, kinetic or kinematic analyses could not produce contact pressure distributions at the knee and ankle cartilage during motion [49–51]. Thus, the proposed method is expected to provide a foundation for evaluating medical aid effects.

There were several limitations in this study. Since forward dynamic analysis is technically difficult to perform using biomechanically accurate FE model, static analysis was employed at major stance phases of the gait, including dynamic effects such as muscle forces, joint angles, and GRF except for the inertial forces. Because the joint angles were specified and rotational DOFs were fixed, it is difficult to see the effect of rotational inertia on the cartilage contact pressure. The OpenSim model we used did not consider medial/lateral degrees of freedom. So, it was difficult to determine the correct relative distribution of medial versus lateral condyle with this model. Only the effect of the geometry changed by the knee angle can be examined, but it could be improved for further research by using the OpenSim model which has higher degrees of freedom at knee. The material properties of cartilages were simplified as elastic to enhance calculation efficiency. Therefore, the analysis results might have an error if large deformation occurs. For a more accurate analysis, ligaments also should be constructed as 3D geometry, and anisotropic hyperelastic material properties should be used for ligaments. Ligaments actually limit the rotation and translation of the joints and also increases cartilage contact pressure according to the changes of joint angle. In this study, the abduction/adduction rotations of the knee were not considered, and the initial length/tension of the ligament was not applied because FE models were reconstructed based on motion data. Therefore, the ligaments were used only to limit joint translation and the effect of increased contact pressure due to initial strain was not considered. According to Shelburne et al., GRF and muscle force are the major factors in articular contact during normal gait. Therefore, it was assumed that ligaments had little effect on the results of the present study. In addition, the ligament model was simplified as a two-node truss element. The results of the contact pressure distribution from the FE analysis are sensitive to the geometry of the biomechanical FE model involved. In this study, the reference model was linearly scaled according to the subject's size, and thus the model was not fully subject specific. The contact pressure distributions at the knee and ankle cartilage were observed simultaneously during the gait while this information is unavailable in other studies. The contact pressure distribution at the cartilage is notable as it is known to be a major factor of cartilage maintenance and degeneration. This is the merit of this study [52,53]. If the lower extremity experiences severe motion such as running and jumping, the stresses in the bone are important for predicting injuries. In such a case, if appropriate material properties of the trabecular and cortical bones are employed, the stresses in bone can be estimated in our proposed method.

5. Conclusions

A new method for the biomechanical analysis of the lower extremity in motion is proposed in this study. Using a FE analysis integrated with a motion analysis, the contact pressure distributions

at the knee and ankle at major stance phases of the gait were assessed. The contact pressures in the human lower extremity were estimated according to gait motions performed by a specific subject. The analysis of the present study is not dynamic. However, it includes external dynamic forces such as the GRF and internal dynamic forces such as active muscle force. The results were more comprehensive compared with previous studies in view of contact pressure distributions at the knee and ankle in motion directly. The present method could be further utilized to offer guidelines for lower-extremity-related products such as shoes or walking aids.

Conflict of interest

The authors declared that they have no competing interests about this study.

Ethical approval

The study was approved by the Korea University Institutional Review Board (Ref. 1040548-KU-IRB-15-263-A-1) and written informed consent obtained from the participant.

Acknowledgments

This work was supported by the National Research Foundation of Korea (NRF) grant funded by the Korea government (MSIP) (NRF-2016R1A2B4013885).

References

[1] Delp SL, Anderson FC, Arnold AS, Loan P, Habib A, John CT, et al. OpenSim: open-source software to create and analyze dynamic simulations of movement. IEEE Trans Biomed Eng 2007;54(11):1940–50.
[2] Huynh K, Gibson I, Jagdish B, Lu W. Development and validation of a discretised multi-body spine model in lifeMOD for biodynamic behaviour simulation. Comput Methods Biomech Biomed Eng 2015;18(2):175–84.
[3] Damsgaard M, Rasmussen J, Christensen ST, Surma E, De Zee M. Analysis of musculoskeletal systems in the anybody modeling system. Simul Model Pract Theory 2006;14(8):1100–11.
[4] Liu MQ, Anderson FC, Schwartz MH, Delp SL. Muscle contributions to support and progression over a range of walking speeds. J Biomech 2008;41(15):3243–52.
[5] Kia M, Stylianou AP, Guess TM. Evaluation of a musculoskeletal model with prosthetic knee through six experimental gait trials. Med Eng Phys 2014;36(3):335–44.
[6] Wang X, Ma Y, Hou BY, Lam W-K. Influence of gait speeds on contact forces of lower limbs. J Healthc Eng 2017;2017:1–6.
[7] Simic M, Wrigley T, Hinman R, Hunt M, Bennell K. Altering foot progression angle in people with medial knee osteoarthritis: the effects of varying toe-in and toe-out angles are mediated by pain and malalignment. Osteoarthr Cartil 2013;21(9):1272–80.
[8] Taniguchi M, Tateuchi H, Takeoka T, Ichihashi N. Kinematic and kinetic characteristics of Masai barefoot technology footwear. Gait Posture 2012;35(4):567–72.
[9] Shelburne KB, Torry MR, Pandy MG. Contributions of muscles, ligaments, and the ground-reaction force to tibiofemoral joint loading during normal gait. J Orthop Res 2006;24(10):1983–90.
[10] Winby CR, Lloyd DG, Besier TF, Kirk TB. Muscle and external load contribution to knee joint contact loads during normal gait. J Biomech 2009;42(14):2294–300.
[11] Cheung JT-M, Zhang M. A 3-dimensional finite element model of the human foot and ankle for insole design. Arch Phys Med Rehabil 2005;86(2):353–8.
[12] Cheung JT-M, Zhang M. Parametric design of pressure-relieving foot orthosis using statistics-based finite element method. Med Eng Phys 2008;30(3):269–77.
[13] Cheung JT-M, Zhang M, An K-N. Effects of plantar fascia stiffness on the biomechanical responses of the ankle–foot complex. Clin Biomech 2004;19(8):839–46.
[14] Cheung JT-M, Zhang M, Leung AK-L, Fan Y-B. Three-dimensional finite element analysis of the foot during standing – a material sensitivity study. J Biomech 2005;38(5):1045–54.
[15] Liu X, Zhang M. Redistribution of knee stress using laterally wedged insole intervention: finite element analysis of knee–ankle–foot complex. Clin Biomech 2013;28(1):61–7.
[16] Gefen A, Megido-Ravid M, Itzchak Y, Arcan M. Biomechanical analysis of the three-dimensional foot structure during gait: a basic tool for clinical applications. J Biomech Eng 2000;122(6):630–9.
[17] Donahue TLH, Hull M, Rashid MM, Jacobs CR. A finite element model of the human knee joint for the study of tibio-femoral contact. J Biomech Eng 2002;124(3):273–80.
[18] Penrose J, Holt G, Beaugonin M, Hose D. Development of an accurate three-dimensional finite element knee model. Comput Methods Biomech Biomed Eng 2002;5(4):291–300.
[19] Ackerman MJ. The visible human project. Proc IEEE 1998;86(3):504–11.
[20] Kiapour A, Kiapour AM, Kaul V, Quatman CE, Wordeman SC, Hewett TE, et al. Finite element model of the knee for investigation of injury mechanisms: development and validation. J Biomech Eng 2014;136(1):011002.
[21] Attarian DE, McCrackin HJ, DeVito DP, McElhaney JH, Garrett Jr WE. Biomechanical characteristics of human ankle ligaments. Foot Ankle 1985;6(2):54–8.
[22] Siegler S, Block J, Schneck CD. The mechanical characteristics of the collateral ligaments of the human ankle joint. Foot Ankle 1988;8(5):234–42.
[23] Corazza F, O'connor J, Leardini A, Castelli VP. Ligament fibre recruitment and forces for the anterior drawer test at the human ankle joint. J Biomech 2003;36(3):363–72.
[24] Butler DL, Kay MD, Stouffer DC. Comparison of material properties in fascicle-bone units from human patellar tendon and knee ligaments. J Biomech 1986;19(6):425–32.
[25] Quapp K, Weiss J. Material characterization of human medial collateral ligament. J Biomech Eng 1998;120(6):757–63.
[26] Momersteeg T, Blankevoort L, Huiskes R, Kooloos J, Kauer J, Hendriks J. The effect of variable relative insertion orientation of human knee bone-ligament-bone complexes on the tensile stiffness. J Biomech 1995;28(6):745–52.
[27] Drake R, Vogl AW, Mitchell AW. Gray's Anatomy for Students E-Book. Elsevier Health Sciences; 2009.
[28] Adouni M, Shirazi-Adl A. Evaluation of knee joint muscle forces and tissue stresses-strains during gait in severe AO versus normal subjects. J Orthop Res 2014;32(1):69–78.
[29] Anderson DD, Goldsworthy JK, Li W, Rudert MJ, Tochigi Y, Brown TD. Physical validation of a patient-specific contact finite element model of the ankle. J Biomech 2007;40(8):1662–9.
[30] Arnold EM, Ward SR, Lieber RL, Delp SL. A model of the lower limb for analysis of human movement. Ann Biomed Eng 2010;38(2):269–79.
[31] Delp SL, Loan JP, Hoy MG, Zajac FE, Topp EL, Rosen JM. An interactive graphics-based model of the lower extremity to study orthopaedic surgical procedures. IEEE Trans Biomed Eng 1990;37(8):757–67.
[32] Rajagopal A, Dembia CL, DeMers MS, Delp DD, Hicks JL, Delp SL. Full-body musculoskeletal model for muscle-driven simulation of human gait. IEEE Trans Biomed Eng 2016;63(10):2068–79.
[33] Osu R, Franklin DW, Kato H, Gomi H, Domen K, Yoshioka T, et al. Short-and long-term changes in joint co-contraction associated with motor learning as revealed from surface EMG. J Neurophysiol 2002;88(2):991–1004.
[34] Mogk JP, Keir PJ. Crosstalk in surface electromyography of the proximal forearm during gripping tasks. J Electromyogr Kinesiol 2003;13(1):63–71.
[35] McDonnell MN, Ridding MC, Flavel SC, Miles TS. Effect of human grip strategy on force control in precision tasks. Exp Brain Res 2005;161(3):368–73.
[36] Nelson-Wong E, Gregory DE, Winter DA, Callaghan JP. Gluteus medius muscle activation patterns as a predictor of low back pain during standing. Clin Biomech 2008;23(5):545–53.
[37] Ivanenko YP, Poppele RE, Lacquaniti F. Five basic muscle activation patterns account for muscle activity during human locomotion. J Physiol 2004;556(1):267–82.
[38] Faux ID, Pratt MJ. Computational geometry for design and manufacture. Ellis Horwood Ltd; 1979.
[39] Briot S, Khalil W. Homogeneous transformation matrix. In: Dynamics of parallel robots. Springer; 2015. p. 19–32.
[40] Shirazi R, Shirazi-Adl A, Hurtig M. Role of cartilage collagen fibrils networks in knee joint biomechanics under compression. J Biomech 2008;41(16):3340–8.
[41] Fukubayashi T, Kurosawa H. The contact area and pressure distribution pattern of the knee: a study of normal and osteoarthrotic knee joints. Acta Orthop Scand 1980;51(1–6):871–9.
[42] Kurosawa H, Fukubayashi T, Nakajima H. Load-bearing mode of the knee joint: physical behavior of the knee joint with or without menisci.. Clin Orthop Rel Res 1980;149:283–90.
[43] Brown TD, Shaw DT. Instantaneous in vitro contact stress distributions on the femoral condyles. J Biomech 1985;18(3):227.
[44] Krause W, Pope M, Johnson R, Wilder D. Mechanical changes in the knee after meniscectomy.. JBJS 1976;58(5):599–604.
[45] Walker PS, Erkiuan MJ. The role of the menisci in force transmission across the knee.. Clin Orthop Rel Res 1975;109:184–92.
[46] Inaba H, Arai M, Watanabe W. Influence of the varus–valgus instability on the contact of the femoro-tibial joint. Proc Inst Mech Eng Part H: J Eng Med 1990;204(1):61–4.
[47] Li G, DeFrate LE, Park SE, Gill TJ, Rubash HE. In vivo articular cartilage contact kinematics of the knee. Am J Sports Med 2005;33(1):102–7.
[48] Komistek RD, Stiehl JB, Dennis DA, Paxson RD, Soutas-Little RW. Mathematical model of the lower extremity joint reaction forces using Kane's method of dynamics. J Biomech 1997;31(2):185–9.
[49] Kakihana W, Akai M, Nakazawa K, Naito K, Torii S. Inconsistent knee varus moment reduction caused by a lateral wedge in knee osteoarthritis. Am J Phys Med Rehabil 2007;86(6):446–54.
[50] Crenshaw SJ, Pollo FE, Calton EF. Effects of lateral-wedged insoles on kinetics at the knee.. Clin Orthop Rel Res 2000;375:185–92.

[51] Maly MR, Culham EG, Costigan PA. Static and dynamic biomechanics of foot orthoses in people with medial compartment knee osteoarthritis. Clin Biomech 2002;17(8):603–10.
[52] Beaupre GS, Stevens SS, Carter DR. Mechanobiology in the development, maintenance, and degeneration of articular cartilage. J Rehab Res Dev 2000;37(2):145.
[53] Carter DR, Beaupré GS, Wong M, Smith RL, Andriacchi TP, Schurman DJ. The mechanobiology of articular cartilage development and degeneration.. Clin Orthop Rel Res 2004;427:S69–77.